Journal of Medicinal Chemistry

pubs.acs.org/jmc

Article

A 5-FU Precursor Designed to Evade Anabolic and Catabolic Drug Pathways and Activated by Pd Chemistry *In Vitro* and *In Vivo*

Published as part of the Journal of Medicinal Chemistry virtual special issue "New Drug Modalities in Medicinal Chemistry, Pharmacology, and Translational Science".

Catherine Adam,[#] Thomas L. Bray,[#] Ana M. Pérez-López, Ee Hong Tan, Belén Rubio-Ruiz, Daniel J. Baillache, Douglas R. Houston, Mark J. Salji, Hing Y. Leung, and Asier Unciti-Broceta*

Cite This: *J. Med. Chem.* 2022, 65, 552−561

Read Online

ACCESS | Metrics & More | Article Recommendations | Supporting Information

ABSTRACT: 5-Fluorouracil (5-FU) is an antineoplastic antimetabolite that is widely administered to cancer patients by bolus injection, especially to those suffering from colorectal and pancreatic cancer. Because of its suboptimal route of administration and dose-limiting toxicities, diverse 5-FU prodrugs have been developed to confer oral bioavailability and increase the safety profile of 5-FU chemotherapy regimens. Our contribution to this goal is presented herein with the development of a novel palladium-activated prodrug designed to evade the metabolic machinery responsible for 5-FU anabolic activation and catabolic processing. The new prodrug is completely innocuous to cells and highly resistant to metabolization by primary hepatocytes and liver S9 fractions (the main metabolic route for 5-FU degradation), whereas it is rapidly converted into 5-FU in the presence of a palladium (Pd) source. *In vivo* pharmokinetic analysis shows the prodrug is rapidly and completely absorbed after oral administration and exhibits a longer half-life than 5-FU. *In vivo* efficacy studies in a xenograft colon cancer model served to prove, for the first time, that orally administered prodrugs can be locally converted to active drugs by intratumorally inserted Pd implants.

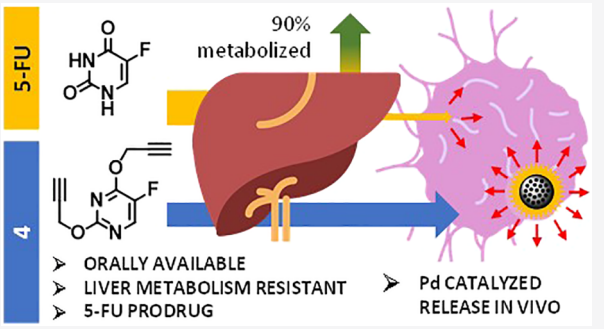

INTRODUCTION

Toxic side effects from cancer chemotherapy are often dose-limiting, and even life-threatening, preventing patients from receiving an optimal treatment regimen. Fluoropyrimidines (Figure 1), which include 5-FU (**1**) and the 5-FU precursors tegafur (**2**) and capecitabine, are among the most prescribed cancer chemotherapies used to treat breast, bowel, skin, stomach, esophageal and pancreatic cancers but can have from moderate to highly serious adverse effects. 5-FU is an antimetabolite drug widely used to treat cancers of the colon and pancreas, alone or in combination,[1,2] that exerts its anticancer effects through the inhibition of thymidylate synthase (TS) and the incorporation of its metabolites into RNA and DNA. Modulation strategies, such as cotreatment with folinic acid, leucovorin, or methotrexate, have been developed to increase the anticancer activity and tolerability of 5-FU. Nevertheless, 5-FU toxicity alone is responsible for numerous deaths each year in the USA.[1,2]

The enzyme dihydropyrimidine dehydrogenase (DPD) is the major detoxifying route for fluoropyrimidines in the liver. DPD reduces 5-FU to 5,6-dihydro-5-fluorouracil in the presence of NADPH. In most of the population, 5-FU is quickly catabolized to this inactive form.[3] However, 3−5% of patients express no or low levels of DPD.[4] As a result, when they are given the standard dose of 5-FU used in most chemotherapy regimens (200−600 mg/m^2), they effectively receive an amount of the drug that is 10-fold higher than the required dose, causing severe adverse effects.[4] *DPYD* genotyping (the DPD encoding gene) or uracil blood testing (uracil is broken down by DPD) prior to treatment with 5-FU, capecitabine, and other analogues is now recommended by the FDA and the EMA.[5,6]

By *ad hoc* chemical design, bioorthogonal prodrugs may offer a way to bypass unwanted and unpredictable side-effects of cancer chemotherapy.[7,8] This class of prodrugs, which are conceptually related to enzyme prodrug therapies (*e.g.*, ADEPT, GDEPT),[9] rely on masking strategies that cannot be activated by the patients' metabolic pathways. Bioorthogonal prodrugs are converted to active drugs by nonbiological stimuli such as abiotic metal catalysis, photoinduced cleavage, or click-to-

Received: October 6, 2021
Published: January 3, 2022

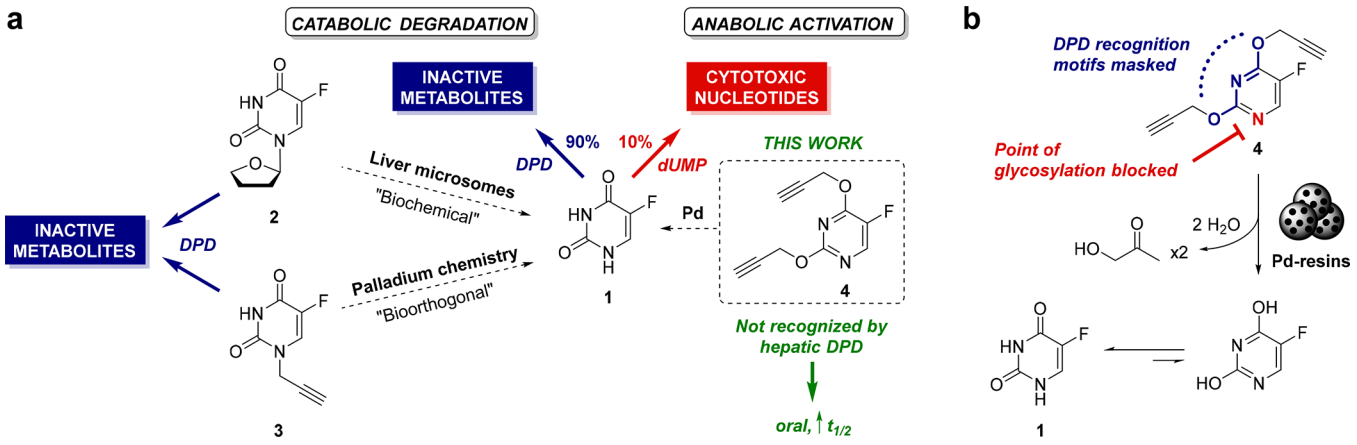

Figure 1. (a) Catabolic and anabolic routes of fluoropyrimidines **1**−**4** *in vivo*. (b) Prodrug **4** is designed to be unrecognized by catabolic DPD and anabolic deoxyuridine monophosphate (dUMP), while it is converted to 5-FU in the presence of Pd catalysts.

release reactions[7,8] and, in principle, can improve suboptimal pharmokinetic (PK) properties of approved therapeutics. The localized generation of cytotoxic compounds at a tumor site using biologically inert precursors and intratumoral catalysts is currently an active area of research, and metal-activated chemotherapy prodrugs for 5-FU,[10,11] doxorubicin,[12−15] floxuridine,[16] gemcitabine,[17] SN-38 (active metabolite of irinotecan),[18] nitric oxide precursors,[19] nitrogen mustard,[20] paclitaxel,[21] and HDAC inhibitors[22−24] have all been reported. Among the catalyst triggers explored in this experimental therapeutic modality are organometallic complexes and nanomaterials based on Ru,[12,25−28] Au,[14,24,29,30] Cu,[31,32] Pt[33] and Pd.[9−11,14−23,34−36]

Our lab has focused on harnessing the remarkable ability of Pd to quickly uncage *N*- and *O*-alkylated compounds in biological settings. To do so, we have developed Pd-loaded microdevices that can be readily implanted in tumors when guided by real-time ultrasound imaging and demonstrated that, after 3 weeks of implantation in growing mouse tumors, the devices can elicit *ex vivo* prodrug activation.[15] Other groups have also shown promising anticancer effects by delivering Pd-containing nanowires or liposomal formulations to tumors and administering bioorthogonal prodrugs by intraperitoneal or intravenous (IV) routes.[11,14] However, the development of prodrugs that are able to address inherent PK issues of approved therapeutics, *e.g.*, low oral bioavailability, and are at the same time activated within the tumor by intratumorally delivered Pd catalysts has not yet been reported. This goal served as the driver for the ligand-based design explored in this work (Figure 1b) to develop a 5-FU prodrug that is orally available, resistant to first-pass metabolism, unaffected by variations in the DPD phenotype, and selectively activated by a bioorthogonal Pd-catalyzed reaction.

RESULTS AND DISCUSSION

Prodrug Design and Synthesis. The lactam tautomer of the pyrimidine ring of 5-FU is key to the molecular recognition of the drug by DPD and other metabolic enzymes (Figure 1a and b). Based on this principle, we rationalized that trapping the structure in its lactim form would render the molecule enzymatically unrecognizable to both catabolic and anabolic 5-FU routes. To achieve this, we decided to investigate the *O,O′*-dipropargylation of 5-FU (Figure 1). This contrasts with the *N*-alkylation strategy previously used by our lab in the development of Pro-5FU (**3**),[10] a Pd-activatable prodrug used as a reference in this study.

To gain preliminary insight into the binding potential of prodrug **4** at the active site of DPD, *in silico* docking studies were performed with **1**, **3**, and **4** in the available crystal structure of DPD.[37] 5-FU (Figure 2a) is predicted to bind with a mode

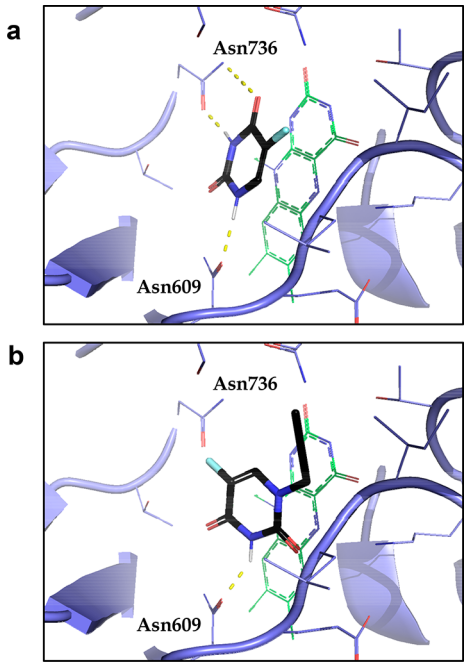

Figure 2. Predicted binding modes of (a) 5-FU (**1**) and (b) Pro-5FU (**3**) within the binding pocket of DPD[37] (PBD 1GTE). Small molecules are represented by sticks where C atoms are black, N atoms are blue, O atoms are red, and polar H and F atoms are white. Protein is colored blue, flavin green, and side chains within 5 Å of the ligands are shown as lines.

identical to that of uracil (Figure S5), accepting H-bonds from Asn609 and Asn736 with an affinity of 206 μM. Pro-5FU (**3**) is also predicted to form a H-bond with Asn609, although its alkyne group induces a rotated binding mode that precludes H-bonding to Asn736 (Figure 2b). Of note, its predicted affinity (87 μM) is higher than that of 5FU, indicating that **3** is as good of a DPD substrate as 5-FU. In contrast to these lactam analogs, docking studies predict that the lactim derivative **4** does not fit into the restricted binding pocket of DPD with an estimated

https://doi.org/10.1021/acs.jmedchem.1c01733
J. Med. Chem. 2022, 65, 552−561

binding affinity of >9000 μM; it is essentially a non-binder in the context of docking.

Encouraged by the *in silico* studies, we carried out the preparation of **4**. This novel 5-FU derivative was synthesized by the reaction of commercially available 5-fluoro-2,4-dichloropyrimidine (**5**) with *in situ* generated propargyl alkoxide, and the *O,O′*-dialkylated derivative **4** was obtained with an 86% yield on a multigram scale (Scheme 1).

Scheme 1. Synthesis of 4[a]

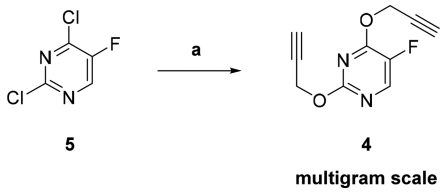

[a]Reagents and conditions are as follows: (a) propargyl alcohol, NaH (60% in mineral oil), THF, 30 min, − 4 °C to rt, then addition of **5**, THF, rt, 12 h.

Pd-Mediated Conversion of 4 into 5-FU. First, the sensitivity of the prodrug to Pd catalysis was tested under physiological conditions. **4** was incubated with Pd resins[15] in PBS at 37 °C, and the conversion to **1** was monitored over time by UPLC (Figure 3). The formation of drug **1** (RT = 0.78 min)

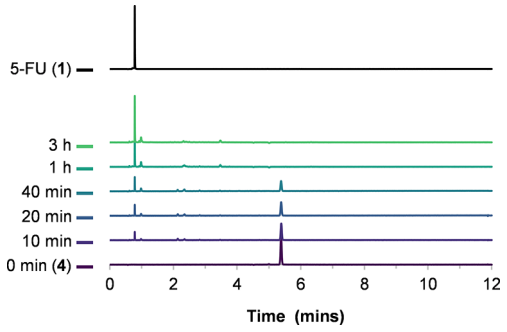

Figure 3. Monitoring the Pd-catalyzed generation of **1** from prodrug **4** (100 μM in PBS), which was shaken at 37 °C with 1 mg/mL Pd resins for 3 h. Full UPLC traces of all time points. Authentic traces of **1** (RT = 0.78 min, top line) and **4** (RT = 5.39 min, bottom line) are shown in black and magenta, respectively.

was observed just after 10 min into the reaction, and the complete disappearance of the peak corresponding to **4** occurred before 1 h. Evidence of a monopropargylated intermediate was detected at a retention time (RT) of 0.98 min (Figure S6a, insert). The conversion kinetics of **4** into 5-FU are remarkable, being the fastest rate observed for any metal-activatable prodrug developed in our lab. Of note, prodrug **3** required >6 h to achieve 50% conversion under the same reaction conditions.[10]

Cell Assays: Biocompatibility and *In Situ* Activation Studies. 5-FU is a drug widely used against multiple indications, including pancreatic cancer (as a combination therapy) and colorectal cancer (as a frontline therapy). Hence, pancreatic cancer BxPC-3 and colorectal cancer HCT116 cells were selected as cell models to test the inherent antiproliferative activity of prodrug **4** (Figure 4a and c, respectively). In agreement with the presumption that a trapped lactim prodrug can not be anabolically activated into the active metabolites of 5-

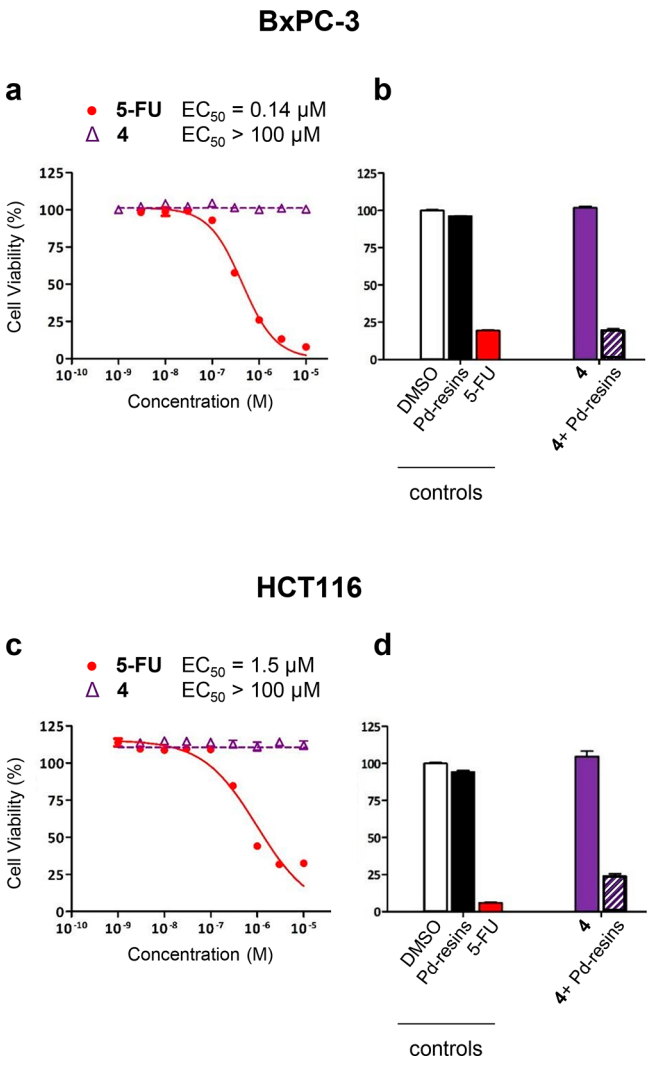

Figure 4. (a and c) Biocompatibility and (b and d) Pd-mediated activation assay of prodrug **4** in a cell culture compared to 5-FU. (a and c) Dose−response curves for BxPC-3 and HCT116 cells after a 5 d treatment with 5-FU and **4**. (b and d) Pd-catalyzed activation of **4**. Experiments were as follows: 0.1% v/v DMSO (untreated cell control, white), 1 mg/mL Pd resins (negative control, black), 5-FU (positive control, red), **4** (negative control, solid purple), and 1 mg/mL Pd resins + **4** (prodrug activation, purple stripes). Concentrations were as follows: 1 μM drug/prodrug for BxPC-3 cells and 3 μM drug/prodrug for HCT116 cells. Cell viability was measured at day 5 using the PrestoBlue reagent. Error bars are ± SD, n = 3.

FU, treatment with prodrug **4** elicited no signs of a cytotoxic effect at any of the concentrations tested (up to 100 μM). In contrast, 5-FU displayed potent anticancer activity, with EC_{50} values of 0.14 and 1.5 μM for BxPC-3 and HCT116, respectively.

Next, prodrug **4** was assessed for activation with Pd resins in the cell culture. Pd resins, **4**, or a combination of both were initially evaluated in BxPC3 cells (Figure 4b) and HCT116 (Figure 4d) cells at 1 and 3 μM, respectively. The combination of **4** and Pd resins displayed a significant cytotoxic effect in both cell lines, whereas neither **4** nor Pd resins individually affected the cell viability. This experiment confirmed the requirement for Pd catalysts to release 5-FU from the trapped lactim analogue **4** and unleash its cytotoxic properties.

https://doi.org/10.1021/acs.jmedchem.1c01733
J. Med. Chem. 2022, 65, 552−561

To evaluate the effect of the different activation rate of the *N*-alkylated prodrug **3**[10] compared to the novel *O,O′*-dialkylated prodrug **4**, we then tested both prodrugs side-by-side at varying concentrations of Pd resins (0.2−1.4 mg/mL) in HCT116 cells (Figure S7). At concentrations of Pd resins above 0.8 mg/mL, the two compounds led to a similar reduction of cell viability. However, the cell viability analysis showed between 7% and 14% higher cell death with compound **4** compared to compound **3** at lower levels of the catalyst (0.8 mg/mL and lower), indicating that the activation rate of the prodrug becomes important when the catalyst concentration decreases.

Drug Metabolism and PK (DMPK) Studies *In Vitro*. To test the metabolic stability of **4** in regard to liver enzymes (including DPD), compounds **1**, **3**, and **4** were incubated with human liver S9 fractions in the presence of NADPH and then analyzed for the presence of 5,6-dihydro-5-fluorouracil (DH5FU)—the reduced and inactive metabolite of 5-FU—by ^{19}F NMR spectroscopy. High levels of DH5FU were seen in reactions with both **1** and **3** (Figure 5b and d, respectively) after

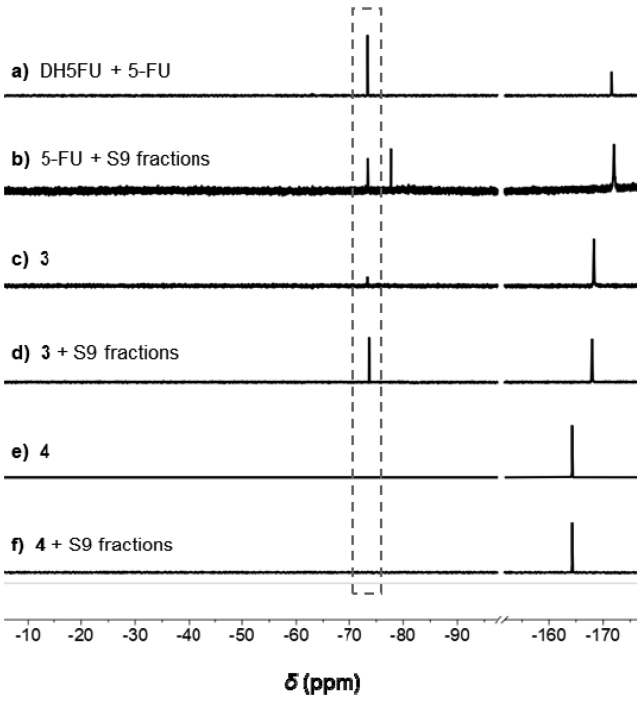

Figure 5. Stability of **1**, **3**, and **4** with S9 liver fractions. ^{19}F-NMR monitoring of the conversion to DH5FU under enzymatic conditions after 1 h. Spectra were recorded at *ca.* 3 mM in DMSO-d_6 at 300 K. The dotted box indicates the region of the expected DH5FU spectra. Experimental conditions were as follows: **1**, **3**, or **4** (1.6 mM); human S9 liver fractions (0.5 mg/mL); and NADPH (1 mM) mixed in PBS at 37 °C for 1 h, 600 rpm. The reaction mixture was quenched (EtOAc) and analyzed by ^{19}F NMR. (a) Control with a mixture of 5-FU (**1**) and an authentic DH5FU sample. (b) Experiment with 5-FU (**1**). (c) Control with a **3** starting solution. (d) Experiment with compound **3**. (e) Control with a **4** starting solution. (f) Experiment with compound **4**.

1 h under enzymatic conditions, with small amounts being visible almost immediately (Figures S8e and S9d). Compound **4**, however, remained completely unaltered under the reaction conditions, suggesting that is stable to liver enzymes (Figure 5f). Compound **4** was also evaluated for metabolic stability to rat liver S9 fractions; again, no DH5FU was observed (Figure S10i).

The stability of compound **4** to primary hepatocytes was next tested to provide further information on the resistance of the compound to first-pass metabolism and hepatic clearance. Rat and human hepatocytes were selected to determine drug clearance in models that represented both the animal of choice for toxicology studies and patients. At a 1 μM concentration of **4**, half-lives of 91 and 322 min were measured in rat and human hepatocytes, respectively (Table 1). This relatively high stability

Table 1. Summary of *In Vitro* DMPK Properties of 4

hepatocyte stability	clint (μL/min/10^6 cells)	$t_{1/2}$ (min)
rat (3 μM)	3.31	418
rat (1 μM)	15.3	91
human (1 μM)	4.51	322
Caco-2 permeability	P_{app} (10^{-6} cm/s)	mean recovery (%)
A to B	28.1 ± 0.697	79.2
B to A	38.8 ± 1.74	73.9
efflux ratio		
P_{app} B2A/P_{app} A2B	1.38	
plasma protein binding	binding (%)	recovery (%)
rat	83.9 ± 1.2	94.8 ± 10.7
human	85.8 ± 0.3	95.7 ± 9.4

to hepatic clearance contrasts with the rapid dealkylation of **4** in the presence of Pd resins (Figure 6), properties that are optimal for a bioorthogonal prodrug.

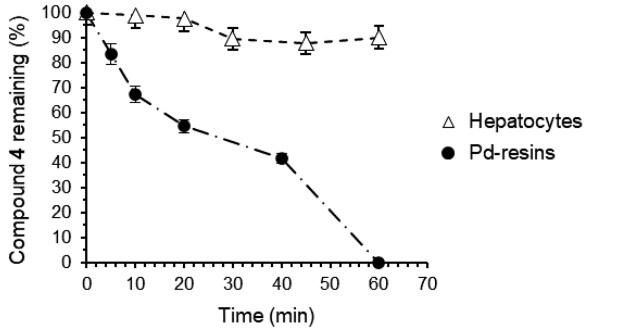

Figure 6. Stability of compound **4** to human primary hepatocytes vs Pd resins at 37 °C. Pd resins: Compound **4** (100 μM in PBS) was incubated with 1 mg/mL Pd resins. Hepatocytes: Compound **4** (10 μM in media) was incubated with 0.5 × 10^6 cells/mL hepatocytes.

The permeation of compound **4** across Caco-2 cell monolayers was measured as a preliminary assessment of the prodrug movement across the intestinal epithelium (Table 1). With an efflux ratio (P_{app}B2A/P_{app}A2B) of 1.38, prodrug **4** does not undergo active efflux. Next, plasma binding of compound **4** (at 5 μM) was quantified in rat and human plasma (Table 1), showing levels of 83.9 ± 1.2% and 85.8 ± 0.3% (n = 3), respectively, and compound recoveries of 94.8 ± 10.7% and 95.7 ± 9.4% (n = 3). Comparatively, *in vitro* human plasma studies that show 5-FU is 10% bound, mainly to albumin.

To identify any potentially active or toxic metabolites resulting from liver metabolism, primary hepatocytes were incubated with 10 μM compound **4** and monitored by LCMS/MS. The parent compound accounted for 95% (rat) and >99% (human) of the related material after 60 min. The only primary metabolites found were trace amounts of each of the mono-*O*-depropargylated isomers (Figures S11), accounting for <5% of the material for rat hepatocytes and <1% of the material for

https://doi.org/10.1021/acs.jmedchem.1c01733
J. Med. Chem. 2022, 65, 552−561

human hepatocytes. Trace amounts of two oxidized metabolites [M + O + 2H] made up <1% of the sample from rat hepatocytes, likely due to oxidation across the triple bonds. Only one of these was detected in the sample from human hepatocytes (see Figures S12 and S13 for LC-MS chromatograms). This study further indicates that **4** was not reduced into inactive metabolites nor transformed into 5-FU by hepatic metabolism.

DMPK Studies *In Vivo*. A pharmacokinetic study of **4** was conducted in rats *via* oral (PO) and IV administration. The IV group (n = 3) was dosed at a concentration of 1 mg/kg and the PO group (n = 3) was dosed at 10 mg/kg. Blood samples were analyzed for the presence of **4** at frequent intervals over 24 h (Figure S14). A summary of the results is shown in Table 2.

Table 2. Summary of DMPK Properties of 4 (rat)

dose (mg/kg)	1[a]	10[a]	1000[b]	1000[b]
route	IV	PO	PO	PO
sex	M	M	M	F
C_{max} (mg/mL)		3.61	84.7	83.6
T_{max} (h)		0.25	1.0	4.0
Cl (mL/min/kg)	52.1			
V_{dss} (L/kg)	1.76			
$t_{1/2}$ (h)	0.497			
AUC_{0-t} (mg/mL*h)	0.324	6.075	1591	1210
AUC_{0-inf} (mg/mL*h)	0.330	6.186	2606	1471
MRT (h)	0.569	1.86	9.70	13.4
bioavailability (% F)		>100 (187)		

[a]*In vivo* DMPK study. [b]Toxicokinetic study.

Highlights of the study are that, contrary to 5-FU, compound **4** exhibits excellent oral bioavailability (>100%). In addition, the half life ($t_{1/2}$) of **4** is 0.497 h (≈30 min), which represents a >6-fold increase relative to that of 5-FU in murine models.[38] Given the ratio observed between the hepatic clearance in human hepatocytes versus that in rat hepatocytes (3.5-fold difference), it an approximate half-life of almost 2 h for prodrug **4** was predicted humans. In patients, the reported elimination half-life of 5-FU is 10−20 min,[39,40] although significant variability was found between different studies.[41]

***In Vivo* Toxicology of Prodrug 4.** Toxicity studies were carried out in male and female rats by giving a single oral dose of 1000 mg/kg **4** (top dose generally used in toxicology studies) in a volume of 10 mL/kg (n = 6). No mortality or abnormal clinical signs resulted over the following 14 d observation period. Body weight slightly decreased between day 2 and day 5 (mainly attributed to two animals), and body weight gain was normal (Figure S15). At necroscopy (day 15), no abnormal macroscopic findings were seen on the organs. Under the experimental conditions, a single dose of **4** at a concentration of 1000 mg/kg did not induce any sign of toxicity in this animal model, which indicates that the novel prodrug design can successfully evade the enzymatic pathways that convert 5-FU into cytotoxic metabolites. With regards to drug exposure, supra-dose proportionality was observed at 1000 versus 10 mg/kg (see Table 2 and Figure S16).

Long-Term Tolerability of the Pd Resins *In Vivo*. As the design of this therapeutic approach hinges on functional, nontoxic, and implantable Pd resins, an assessment of the safety of the devices was performed in rats over a long period of time. Rats were implanted subcutaneously with Pd resins, and skin samples underwent histopathological examination after 1, 3, 7, 28, and 84 d (n = 3 per time point, plus one control with no Pd resins). Over the course of the study, the implanted devices were well-tolerated clinically and remained present and intact. No changes in body weight or temperature compared to those of the controls were observed in the rats. Blood hematology showed no changes in blood parameters over the three-month period. A slight-to-moderate granulomatous inflammatory reaction was present around the implanted devices in all rats, peaking at day 28, and a fibrous capsule was noted around the devices on all animals (see the representative image at day 84 in Figure 7).

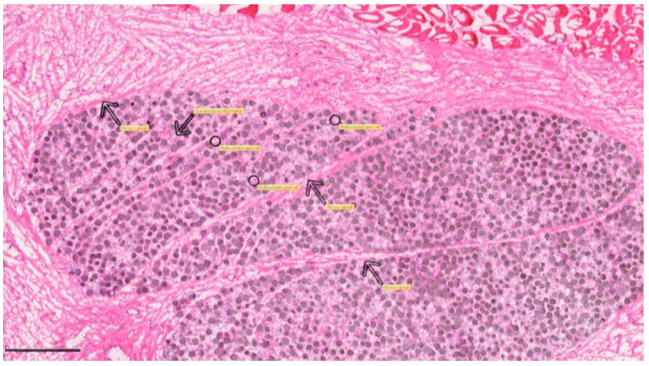

Figure 7. Representative H&E-stained histology image of a rat dermis after 84 days implantation with Pd resins. Image shows the presence of a cavity of discrete-to-marked size in the subcutaneous tissue containing the Pd resins (round, greyish material) and surrounded by a fibrous capsule (indicated by arrows).

None of these microscopic changes were considered clinically significant but were associated with a standard foreign body reaction toward the implanted material, circumscribed by a fibrous capsule, suggesting a locally constrained inflammatory process.

Tolerability Study in Mice Bearing HCT116 Tumors. Following best practice guidance,[42] rodent toxicology studies were performed in the rats. However, to test the efficacy of the therapeutic strategy *in vivo*, we used a human HCT116 xenograft model in mice, as this animal model is well-established in our lab. Before this, a preliminary study was performed to evaluate the tolerability of the intratumoral injection of Pd resins in combination with the daily oral administration of prodrug **4** (Figure S17a). Nude mice were subcutaneously inoculated with HCT116 cells (500 000 cells/mouse), and tumors were left to grow to a size of 0.2−0.3 cm^3 (measured by caliper). Mice were randomized in four groups (n = 4), one of which remained untreated (group 4). The Pd resins were inserted into tumors of the rest of the groups by intratumoral injection (2 mg per 50 μL/mouse). Mice were treated daily by oral gavage for seven days with the vehicle (group 3) or 75 (group 2) or 150 mg/kg **4** (group 1). No macroscopic clinical signs, including a loss of body weight (Figure S17b), were observed during the treatment phase. Plasma analysis showed very low levels of 5FU were released to the bloodstream. Of note, high levels of brain penetration were observed for prodrug **4** (Figure S17c), a further indication of its excellent distribution properties. The study concluded that daily doses of the prodrug **4** at a concentration of 150 mg/kg were well-tolerated in mice containing subcutaneous tumors with implanted Pd resins.

***In Vivo* Efficacy Study in Mice Bearing HCT116 Tumors.** Building on the tolerability studies, daily oral doses of 150 mg/kg prodrug **4** were selected to study local chemotherapy activation by intratumorally implanted Pd resins in a

https://doi.org/10.1021/acs.jmedchem.1c01733
J. Med. Chem. 2022, 65, 552−561

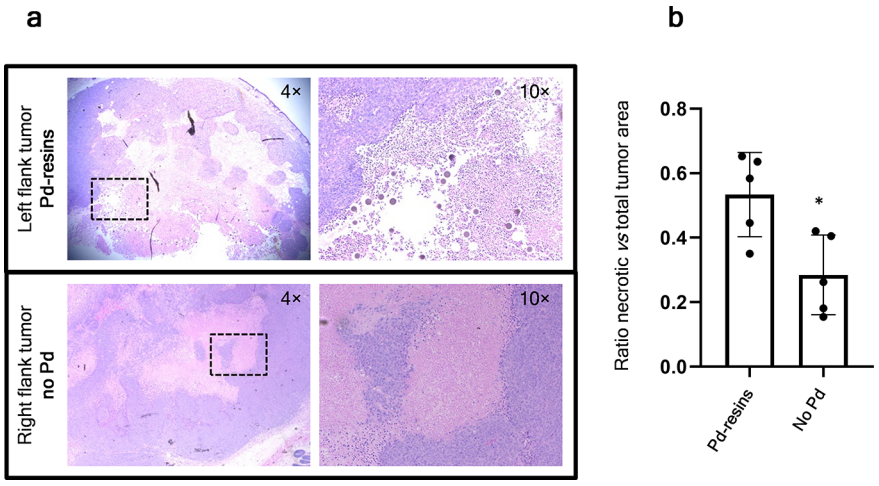

Figure 8. (a) Representative H&E HCT116 tumor sections from mice treated with prodrug **4**. (Top) Left flank tumor (implanted with 2 mg of Pd resins). (Bottom) Right flank tumor (injected with the vehicle). (b) Analysis of the ratio of necrotic tissue vs the total HCT116-tumor area between left and right flank tumors. $n = 5$, $^*p = 0.0317$ (Mann−Whitney Test).

subcutaneous HCT116 colorectal cancer xenograft model (Figure S18a). To evaluate the impact of the presence and absence of Pd resins in the same animal, mice ($n = 5$) were inoculated with HCT116 cells in both flanks. After tumors reached a size of 0.2−0.3 cm^3 (day 26), Pd resins were implanted in the left tumor and only the vehicle (PBS) was implanted in the right tumor. Mice were treated with **4** (150 mg/kg) for 14 consecutive days. Although no differences in the measured mass volume were observed between the tumors at the end point (Figure S18b and c), the histological examination of the tumor samples revealed that the tumors containing Pd devices showed large central necrotic areas in the vicinity of the resins, indicating that 5-FU had been generated inside the tumor and elicited an intratumoral cytotoxic effect (Figure 8a and Figure S19). In contrast, the tumors without Pd resins in the same animal only showed minimal evidence of necrosis, as expected by the physical damage from the control injection of PBS solution. Analysis of the ratio of necrotic tissue versus the total tumor areas between the left (inoculated with Pd resin) and right (inoculated with PBS) tumors show statistically significant differences (Figure 8b), indicating that the Pd resin-injected tumors were able to generate 5-FU locally and cause drug-induced cancer cell death.

CONCLUSIONS

In our search to improve chemotherapy regimens by controlling where and when anticancer drugs are released, we have developed an orally bioavailable precursor of 5-FU that is selectively activated by Pd catalysis. To circumvent the drug's metabolization routes (both anabolic activation and catabolic processing), the novel prodrug was locked in a lactim-type structure by alkylating the O atoms of 5-FU. This masking strategy resulted in an increased stability to DPD-mediated degradation and hepatic clearance, thereby improving *in vivo* DMPK properties relative to 5-FU. Importantly, we show that the release of the free-to-tautomerize drug is only achieved by the reaction with Pd resins. Finally, we show for the first time that an inactive drug precursor can be administered orally and activated inside a tumor xenograft by intratumorally implanted Pd catalysts. Although there is still room to improve the performance and delivery of the metal activator, and the posology of the treatment, this work demonstrates that bioorthogonal strategies can be used not only to improve the tolerability of approved therapeutics but also to solve inherent PK issues of those drugs.

EXPERIMENTAL SECTION

General. Chemicals and reagents were purchased from Sigma-Aldrich and Alfa-Aesar. Flash column chromatography was performed with silica gel (220−440 mesh). NMR spectra were recorded on a Bruker 500 MHz spectrometer at 300 K and referenced relative to the solvent residual peaks with chemical shifts (δ), reported in parts per million. Multiplicity is reported as follows: s, singlet; d, doublet. Coupling constants (J) are shown in hertz. HRMS was obtained using a Bruker 3.0 T Apex II spectrometer under electron spray ionization conditions. Compound **4** used in the biological experiments was >95% pure by HPLC, which was measured usinga Waters 600E (100 μL) gradient pump with a 717 plus autosampler and a Waters 996 Photodiode ArraydDetector (210−400 nm) equipped with a Phenomenex Luna C18(2 (5 μm, 250 × 4.6 m)m column at a flow rate of 1 mL/min with an injection volume of 10 μL. The method was as follows: eluent A, water with TFA (0.1%); eluent B, acetonitrile with TFA (0.1%); A/B = 95:5 to 5:95 in 30 min, 5:95 isocratic 5 min, 5:95 to 95:5 in 5 min, and 95:5 isocratic 10 min.

Synthesis of 2,4-Bis(propargyloxy)-5-fluoro-pyrimidine (4). NaH (60% dispersion in mineral oil) (6.2 g, 155 mmol, 5 equiv) was added to dry THF (100 mL) at 4 °C, and the mixture was stirred rapidly for the dropwise addition of propargyl alcohol (6 mL, 103 mmol, 3.3 equiv) in dry THF (30 mL) over 30 min. An evolution of gas was observed with a slight exothermic reaction, then the flask was sealed and flushed with nitrogen. 5-Fluoro-2,4-dichloropyrimidine (5.1 g, 30.1 mmol 1 equiv) in dry THF (30 mL) was added to the mixture dropwise at rt, and the reaction mixture was stirred for 12 h. The resulting mixture was partitioned between CH_2Cl_2 (250 mL) and H_2O (250 mL) and acidified with acetic acid to pH 3.5, and the aqueous layer was extracted with CH_2Cl_2 (3 × 100 mL). The combined organic phases were concentrated under reduced pressure, and the crude was purified via flash chromatography (10−40% EtOAc/*n*-Hexane) to yield **4** as a white solid (5.5 g, 26.7 mmol, 86.7% yield): ^{1}H NMR (500 MHz, $CDCl_3$) δ 8.14 (d, $J_{H-F} = 2.3$ Hz, 1H), 5.07 (d, $J = 2.4$ Hz, 2H), 4.95 (d, $J = 2.4$ Hz, 2H), 2.54 (t, $J = 2.4$ Hz, 1H), 2.47 (t, $J = 2.4$ Hz, 1H). ^{19}F NMR (376 MHz, DMSO-d_6) −164.3. ^{13}C NMR (126 MHz, $CDCl_3$) 158.5 (C), 158.4 (C), 143.2−142.2 (d, $J_{C-F} = 255.4$ Hz C), 144.2−143.9 (d, $J_{C-F} = 20.6$ Hz CH), 78.3 (C), 77.4 (C) 76.2 (CH), 75.0 (CH), 55.7 (CH2), 55.1 (CH2). HRMS (m/z) $[M + H]^+$ calcd for $C_{10}H_7FN_2O_2$ $[M + H]^+$: 207.0564. Found: 207.0561. Purity: 99.5% (HPLC, Figure S4).

***In Silico* Docking Calculations.** Crystal structures of DPD were examined for their suitability for docking. Chain D of PDB 1GTE was

https://doi.org/10.1021/acs.jmedchem.1c01733
J. Med. Chem. 2022, 65, 552−561

selected to represent DPD as it contained a small-molecule ligand very similar to the compounds to be docked. This structure had been determined with high resolution (1.65 Å).[37] Water molecules and other heteroatoms were removed from the structures, and the program PDB 2PQR 2.1.1[43] was used to assigned position-optimized H atoms, utilizing the additional PropKa[44] algorithm with a pH of 7.4 to predict the protonation states. The MGLTools 1.5.6[43] utility prepare_receptor4.py was used to assign Gasteiger charges to atoms. H atoms were assigned to compound structures using OpenBabel 2.4.1,[45] utilizing the −p option to predict the protonation states of functional groups at pH 7.4. The MGLTools utility prepare_ligand4.py was used to assign Gasteiger charges and rotatable bonds. Autodock 4.2.6[46] was used to automatically dock the compounds into the ATP binding pocket of the crystal structures. A grid box that encompassed the maximum dimensions of the cognate ATP ligand plus 12 Å in each direction was used. The starting translation and orientation of the ligand and the torsion angles of all rotatable bonds were set to random. The autogrid grid point spacing was set at 0.2 Å. The autodock parameter file specified 50 Lamarckian genetic algorithm runs, 15 000 000 energy evaluations, and a population size of 300. The cognate ligand present in the crystal structure (uracil) was successfully redocked as a positive control (Figure S5). Authors will release the atomic coordinates upon article publication.

Pd-Mediated Prodrug Activation *In Vitro*. Prodrug-into-drug conversion was carried out at 37 °C in an isotonic solution with a physiological pH of 7.4. Prodrug **4** (100 μM in PBS) was combined with 1 mg/mL Pd resins (30 μm diameter), and the mixture was shaken at 1200 rpm and 37 °C in a Thermomixer. Reaction crudes were monitored at 10 min, 20 min, 40 min, 1 h, 3 h, 6 h, 24 h, and 48 h by analytical UPLC (Waters Acquity UPLC System) using an Acquity UPLC BEH C18 (1.7 μm, 2.1 × 50 mm) column, T = 60 °C, a flow rate of 0.2 mL/min, and the UV detector at 254 nm. The UPLC method is as follows: eluent A, water and trifluoroacetic acid (0.1%); eluent B, acetonitrile; A/B = 95:5 isocratic 0.5 min, A/B = 95:5 to 5:95 in 10 min, isocratic 0.5 min, 5:95 to 95:5 in 0.1 min, and isocratic 1 min.

Cell Culture. Cell lines were grown in culture media supplemented with 10% fetal bovine serum (FBS) and 2 mM L-glutamine, then incubated in a tissue culture incubator at 37 °C and 5% CO_2. Human colorectal cancer cells HCT116 (purchased from ECACC) were cultured in McCoy's 5A medium. Human pancreas adenocarcinoma BxPC-3 cells (a gift from Dr Mark Duxbury, UoE) were cultured in Roswell Park Memorial Institute (RPMI) media.

Biocompatibility Assays. Cells were seeded in a 96-well plate format at a density of 3000 cells/well for HCT116 and a density of 2500 cells/well for BxPC-3 cells, then incubated for 48 h before treatment. Each well was then replaced with fresh media containing the drug or prodrug and incubated for 5 d. Untreated cells were incubated with DMSO (0.1% by volume). The PrestoBlue cell viability reagent (10% v/v) was added to each well, and the plate was incubated for 1 h. Fluorescence emission was detected using a PerkinElmer Victor2 multilabel reader (excitation filter at 540 nm and emissions filter at 590 nm). All conditions were normalized to the untreated cells (100%), and curves were fitted with GraphPad Prism 5 using a sigmoidal variable slope curve.

Pd-Mediated Prodrug Activation in Cell Culture. Cells were plated as described as above and incubated for 48 h prior to treatment. Wells were then replaced with fresh media containing DMSO (0.1% v/v), Pd resins (1 mg/mL), 5-FU(positive control) or **4** (negative control), and both Pd resins and **4** (activation assay). HCT116 colorectal cancer cells incubated with 3 μM 5-FU or **4** and BxPC-3 pancreatic cancer cells incubated with 1 μM 5-FU or **4**. All wells contained 0.1% v/v DMSO. All cells were incubated with drugs for 5 d. Cell viability and fluorescence emission were detected as above, and results were normalized to the untreated cells (100%).

Pd Resin Dilution Study. HCT116 cells were seeded in a 96-well plate format at a density of 750 cells/well and incubated for 48 h before treatment. Each well was then aspirated and fresh media (95 μL) or fresh media containing Pd resins (20−160 μg in 95 μL) for prodrug activation, and the Pd control wells were added. The compound of interest (5 μL in 2% v/v DMSO/medium at 2 mM) or DMSO (5 μL at 2% v/v) was then added to each well, and cells were incubated for 5 d. Cell viability and fluorescence emission were detected as above, and results were normalized to the untreated cells (100%) for each dilution experiment.

Metabolic Stability Study *In Vitro*. Human and rat (Sprague−Dawley) liver S9 fractions were purchased from ThermoFisher and thawed, aliquoted, and stored at −80 °C upon receipt. DH5FU was purchased from Cambridge BioScience, and 5-FU was purchased from Sigma-Aldrich. Human and rat liver S9 fractions (20 μL at 20 mg/mL) were defrosted slowly over ice and diluted with PBS (732 μL). Compound **1**, **3**, or **4** (8 μL at a concentration of 150 mM in DMSO-d_6) was added, and the mixture preincubated at 37 °C for 5 min. An aliquot of 380 μL of the reaction mixture was removed and incubated for 1 h at 37 °C (control, no NADPH). To the remaining 380 μL was added NADPH (20 μL at 20 mM in PBS). The reaction mixture was mixed, then a 100 μLaliquot was immediately removed and the reaction was stopped (control, t = 0). The remainder (300 μL) was incubated 1 h at 37 °C (experiment). For control experiments in the absence of enzymes, compound **1**, **3**, or **4** (4 μL at a concentration of 150 mM in DMSO-d6) was diluted with PBS (366 μL) and to the solution was added either NADPH (20 μL at 20 mM in PBS, control−no enzymes) or PBS (20 μL control−no enzymes, no NADPH). The reaction mixtures were incubated for 1 h at 37 °C. All reactions were stirred at 600 rpm and stopped by the addition of EtOAc (200 μL), then dried under a stream of N_2. Dried reaction contents were taken up in DMSO-d_6 (400 μL), vortexed for 30 s, centrifuged for 5 min, and analyzed by ^{19}F NMR for the presence of DH5FU by comparison with an authentic sample as purchased (Figure S8g, peak at −73 ppm, indicated by dotted black line).

Permeability Assay. The Caco-2 permeability assay was undertaken by Cytoprex Ltd. Cell culture and assay incubations ware carried out at 37 °C, 5% CO_2, and a relative humidity of 95%. Caco-2 cells (purchased from ATCC, P40-60) were seeded onto Millipore Multiscreen Transwell plates at a desnity of 1 × 10^5 cells/cm^2 and cultured in DMEM. On day 20, the monolayers were prepared by rinsing both apical and basolateral surfaces twice with Hanks Balanced Salt Solution (HBSS, pH 7.4), then incubated with HBSS in both apical and basolateral compartments for 40 min to stabilize the physiological parameters. For the assessment of A−B permeability, HBSS was removed from the apical compartment and replaced with the HBSS solution of compound **4** (10 μM, 1% v/v DMSO). The apical compartment insert was then placed into a companion plate with fresh buffer (containing 1% v/v DMSO). For the assessment of B−A permeability, HBSS was removed from the companion plate and replaced with the HBSS solution of compound **4** (10 μM, 1% v/v DMSO). Fresh buffer (containing 1% v/v DMSO) was added to the apical compartment insert, then placed into the companion plate. The integrity of the monolayer throughout the experiments was checked by monitoring the permeation of lucifer yellow (included in dosing solutions) using fluorometric analysis, and no permeation was observed. After 120 min, the apical compartment inserts and the companion plates were separated, and the apical and basolateral samples were diluted in HBSS with 1% v/v DMSO for analysis. Control compounds (atenolol, propranolol, and talinolol) were run as controls on each assay plate. Compound **4** and control compounds were quantified by LC-MS/MS cassette analysis using an eight-point calibration. The starting concentration (C_0) was determined from the dosing solution, and the experimental recovery was calculated from C_0 and both apical and basolateral compartment concentrations.

Metabolic Stability Study In Cells. Hepatocyte Stability assays were undertaken by Cytoprex Ltd. Compound **4** (3 μM, 0.25% v/v DMSO) in Williams E media supplemented with 2 mM L-glutamine and 25 mM HEPES was preincubated at 37 °C prior to the addition of a suspension of hepatocytes (0.5 × 10^6 cells/mL in Williams E media supplemented with 2 mM L-glutamine and 25 mM HEPES). The total volume was 500 μL. Two control compounds were included alongside the DMSO control. The reactions were stopped by transferring 50 μL of the incubate to 100 μL of methanol containing the internal standard at the appropriate time points. The termination plates were centrifuged at

https://doi.org/10.1021/acs.jmedchem.1c01733
J. Med. Chem. 2022, 65, 552−561

2500 rpm at 4 °C for 30 min to precipitate the protein. Quantitative analysis of the supernatants was performed using LC-MS/MS.

Metabolite profiling was undertaken by Sygnature Discovery Ltd. Compound **4** (10 μM) was separately incubated with rat (Sprague−Dawley, male, BioreclamationIVT) and human (Caucasian, male, Corning) species of cryopreserved hepatocytes (0.5×10^6 cells/mL) in Leibovitz buffer, with a total volume of 330 μL. The reaction was incubated at 37 °C with shaking (700 rpm) for 60 min. Samples were taken at 0 and 60 min, quenched 1:1 with ice-cold acetonitrile, and centrifuged for 15 min, then the supernatant was analyzed using a Waters Xenvo-G2-XS-TOF mass spectrometer with a Waters Acquity UPLC system. Negative controls, hepatocytes only and compound **4** in buffer alone, were run to ensure the detected peaks were compound-related, rather than endogenous to the hepatocytes, and that they corresponded to compound **4** metabolism rather than compound instability under experimental conditions. Positive control incubations were carried out with verapamil (0.5 μM) and 7-hydroxycoumarin (2 μM) to test the viability of the hepatocytes. Chromatography was performed on an Acquity UPLC HSS C18 column (18 μm, 2.1 mm × 100 mm) with a flow rate of 0.45 mL/min and a column temperature of 40 °C. The method is as follows: eluent A, water with TFA (0.1%); eluent B, acetonitrile with TFA (0.1%); A/B = 95:5 isocratic 10 s, 95:5 to 50:50 in 10 min 40 s, 50:50 to 5:95 in 1 min 10 s, 5:95 isocratic 1 min 50 s, 5:95 to 95:5 in 35 s, and 95:5 isocratic 35 s. Samples were analyzed using a Waters Xevo-G2-XS-TOF mass spectrometer with Waters Acquity UPLC system. Full scan spectra were acquired using the MEE method in the positive ion mode for the comparison of low- and high-collision-energy spectra.

In vivo PK studies were performed by Sygnature Discovery Ltd. Seven male jugular vein cannulated rats (Wistar Han, Charles River) were dosed on day 0 with compound **4**; three were dosed intravenously (IV route), three were dosed orally (PO route), and one animal received no intervention (control). Rats weighed between 263 and 319 g and were individually housed. The IV route was as follows: 1 mg/kg administered by dosing 2 mL/kg of a 0.5 mg/mL solution in 5% DMSO/95% HPCD (20% w/v). Food was not withheld overnight. The PO route was as follows: 10 mg/kg administered by dosing 5 mL/kg of a 2 mg/mL suspension in 5% DMSO/95% 0.1% tween 80/99.9% HPCD (0.5% w/v). Food was withheld overnight, and animals were fed after 4 h of sample. The control was as follows: No overnight food withdrawal. Blood samples (2 × 100 μL) were taken at 0.083 (IV route), 0.25, 0.5, 1, 2, 3 (PO route), 4, 6, 8, and 24 h in serial *via* jugular vein cannula. Blood was held on ice for <30 min before transferring 2 × 100 μL to 96-well plates, freezing it on dry ice, and storing at −20 °C. For the anticoagulant, 150 μL of blood was mixed with 150 μL heparinized wate;. 100 μL of the dose formulation samples were also retained. Samples were quantitatively analyzed (QToF) for compound **4** against a calibration curve.

Single-Dose MTD Study. Performed by Sygnature Discovery Ltd. Six animals were treated once by the oral route at 1000 mg/kg, then observed for 14 consecutive days. Morbidity and mortality checks were performed twice daily. General clinical observations were performed before the first administration, twice on the day of treatment (at 1 h ± 30 min postdose and then again between 3 and 4 h postdose), then daily from d2 to d14. Functional and neurobehavioral tests (FOB) were performed on d1 (between 30 min and 2 h post dose), on d7, or on d14. Body weight was recorded on d1, d2, d5, d8, d11, and d14. Animals were killed and subjected to gross necropsy on d15.

Long-term Safety Assessment of Pd Resins Implanted in Rats. The *in vivo* Pd resin study was performed by Evotec. The objective was to perform a histopathological examination of skin samples from male Sprague−Dawley rats at various time points after the subcutaneous implantation of Pd resins. A total of 20 male Sprague−Dawley rats were allocated, and 15 of them were subcutaneously implanted at d0 in the interscapular area with Pd resins (10 mg of Pd devices in 250 μL of sterile PBS, sonicated for 10 min prior to injection with a standard 1 mL syringe fitted with a 9-gauge needle), whereas five control animals stayed naïve. All animals were deeply anesthetized with isoflurane and sacrificed by exsanguination at day 1, 3, 7, 28, or 84 post-implantation. Animals were examined visually for external abnormalities, including palpable masses. Organs from the peritoneal cavity (liver, kidneys, gastro-intestinal tract, spleen, and bladder) and then those from the thoracic cavity (heart and lungs) were observed. Dorsal skin at the implantation site (skin and muscle) was sampled and placed in a plastic mold filled with OCT (Optimal Cutting Temperature compound, Tissue Tek, Sakura). The mold was soaked in an isopentane tank (ca. −70 °C) for few min. Before cutting, the tissue was released from the mold and fixed on the freeze microtome with a drop of OCT. Then, 5 μm sections were obtained with a cryomicrotome (Cryostar NX70, Microm), which were fixed immediately with cold acetone for 10 min and hydrated in TBS for 10 min. Slides were stained with hematoxylin and eosin (H&E). All these steps were performed in a stainer (Tissue-Tek Prisma, Sakura). One section of skin per animal was elected for the histopathological examination. The slides were digitalized with a Hamamatsu Nanozoomer device.

Tolerability Study in Mice Bearing HCT116 Tumors. The tolerability study in mice was performed by Evotec. Fifteen Balbc nude mice (females), 6−7 weeks old from the Janvier laboratory (France), were injected subcutaneously with 5×10^5 HCT116 colorectal cancer cells in 1/2 Matrigel/PBS. Body weight and tumor growth were evaluated weekly until the mean tumor volume reached 200−300 mm^3. Mice were randomized into four groups to receive the following treatments: group 1:, Pd resins and **4** at a concentration of 150 mg/kg ($n = 4$); group 2, Pd resins and **4** at a concentration of 75 mg/kg ($n = 4$); group 3, Pd resins alone and vehicle ($n = 3$); group 4, not treated ($n = 4$). For 7 consecutive days following the injection of Pd resins into tumors (groups 1−3), mice were dosed orally (vehicle, 150 mg/kg, 75 mg/kg, and no treatment for groups 1−4, respectively). Behaviors and clinical signs were checked twice daily, and body weight was checked once daily. Blood samples from each mouse were collected by microsampling on day 7 of treatment, 2 h post administration. Collected plasma was frozen at −20 °C.

***In Vivo* Activation of 4 by Pd Devices.** Five CD-1 nude mice (6−8 weeks) were injected subcutaneously on both flanks with 3×10^6 HCT116 colorectal cancer cells in PBS. Pd resins or the PBS vehicle solution were injected intratumorally when the tumor volume reached 200−300 mm^3. Mice were then dosed orally with 150 mg/kg prodrug **4** for 14 consecutive days following implantation.

■ ASSOCIATED CONTENT

Supporting Information

The Supporting Information is available free of charge at https://pubs.acs.org/doi/10.1021/acs.jmedchem.1c01733.

Methods, spectral, analytical data, molecular formula strings, enzymatic conditions, cell culture, and *in vivo* protocols (PDF)

SMILES data strings (CSV)

5-FU (**1**) docked in 1GTE (PDB)

Pro-5FU (**3**) docked in 1GTE (PDB)

Uracil docked in 1GTE (PDB)

■ AUTHOR INFORMATION

Corresponding Author

Asier Unciti-Broceta − *Cancer Research UK Edinburgh Centre, Institute of Genetics and Cancer, University of Edinburgh, EH4 2XU Edinburgh, U.K.;* orcid.org/0000-0003-1029-2855; Email: Asier.Unciti-Broceta@igmm.ed.ac.uk

Authors

Catherine Adam − *Cancer Research UK Edinburgh Centre, Institute of Genetics and Cancer, University of Edinburgh, EH4 2XU Edinburgh, U.K.*

Thomas L. Bray − *Cancer Research UK Edinburgh Centre, Institute of Genetics and Cancer, University of Edinburgh, EH4 2XU Edinburgh, U.K.;* Present Address: Oxford Nanopore

Technologies, Gosling Building, Edmund Halley Road, Oxford Science Park, Oxford OX4 4DQ, U.K

Ana M. Pérez-López − *Cancer Research UK Edinburgh Centre, Institute of Genetics and Cancer, University of Edinburgh, EH4 2XU Edinburgh, U.K.;* Present Address: Technische Universität Berlin, Institut für Biotechnologie, Aufgang 17-1, Level 4, Raum 472, Gustav-Meyer-Allee 25, 13355 Berlin, Germany.; orcid.org/0000-0002-3900-3335

Ee Hong Tan − *Institute of Cancer Sciences, University of Glasgow, Bearsden, Glasgow G61 1QH, U.K.; Cancer Research UK Beatson Institute, Garscube Estate, Bearsden, Glasgow G61 1BD, U.K.*

Belén Rubio-Ruiz − *Cancer Research UK Edinburgh Centre, Institute of Genetics and Cancer, University of Edinburgh, EH4 2XU Edinburgh, U.K.;* Present Address: GENYO, Centre for Genomics and Oncological Research, Pfizer-University of Granada-Andalusian Regional Government, Parque Tecnológico de la Salud (PTS Granada), Avenida de la Ilustración 114, 18016 Granada, Spain, and Department of Medicinal and Organic Chemistry, Faculty of Pharmacy, University of Granada, Campus de Cartuja S/N, 18071 Granada, Spain.; orcid.org/0000-0003-4720-6578

Daniel J. Baillache − *Cancer Research UK Edinburgh Centre, Institute of Genetics and Cancer, University of Edinburgh, EH4 2XU Edinburgh, U.K.;* orcid.org/0000-0003-0859-829X

Douglas R. Houston − *Institute of Quantitative Biology, Biochemistry and Biotechnology, University of Edinburgh, Edinburgh EH9 3BF, U.K.;* orcid.org/0000-0002-3469-1546

Mark J. Salji − *Institute of Cancer Sciences, University of Glasgow, Bearsden, Glasgow G61 1QH, U.K.; Cancer Research UK Beatson Institute, Garscube Estate, Bearsden, Glasgow G61 1BD, U.K.*

Hing Y. Leung − *Institute of Cancer Sciences, University of Glasgow, Bearsden, Glasgow G61 1QH, U.K.; Cancer Research UK Beatson Institute, Garscube Estate, Bearsden, Glasgow G61 1BD, U.K.*

Complete contact information is available at: https://pubs.acs.org/10.1021/acs.jmedchem.1c01733

Author Contributions

#Equal contribution.

Notes

The authors declare the following competing financial interest(s): The authors declare that compound 4 was protected under patent application PCT/GB2017/051379.

■ ACKNOWLEDGMENTS

We are grateful to the EPSRC (EP/N021134/1) for funding. T.L.B. thanks the CMVM of the University of Edinburgh (Principal's scholarship), and B.R.-R. thanks the EC (H2020-MSCA-IF-2014-658833, ChemoBOOM) for financial support. A.U.-B. and D.J.B. thank Medical Research Scotland (PHD-1046-2016) for funding. We acknowledge support from the MRC Confidence in Concept scheme (MRC/CIC6/52) and EPSRC Impact Acceleration Account (PIII024).

■ ABBREVIATIONS

5-FU, 5-fluorouracil; ADME, absorption, distribution, metabolism, and excretion; d, day; DH5FU, 5,6-dihydro-5-fluorouracil; DMPK, drug metabolism and pharmacokinetics; DMSO, dimethyl sulfoxide; DPD, dihydropyrimidine dehydrogenase; dUMP, deoxyuridine monophosphate; EtOAc, ethyl acetate; eq, equivalents; ESI, electronic Supporting Information; h, hours; HE, hematoxylin and eosin; HPCD, hydroxypropylmethyl cellulose; HPLC, high-performance liquid chromatography; HRMS, high-resolution mass spectrometry; IV, intravenous; LC-MS, liquid chromatography−mass spectrometry; min, minutes; NADPH, nicotinamide adenine dinucleotide phosphate; NMR, nuclear magnetic resonance; PBS, phosphate-buffered saline; PK, pharmacokinetic; PO, per os; RT, retention time; rt, room temperature; s, seconds: SD, standard deviation; TBS, tris-buffered saline; THF, tetrahydrofuran; TS, thymidylate synthase; TFA, trifluoroacetic acid; UPLC, ultra performance liquid chromatography

■ REFERENCES

(1) von Borstel, R.; O'Neil, J. D.; Saydoff, J. A.; Bamat, M. K. Uridine triacetate for lethal 5-FU toxicity due to dihydropyrimidine dehydrogenase (DPD) deficiency. *J. Clin. Oncol.* **2010**, *28*, No. e13505.

(2) Sara, J. D.; Kaur, J.; Khodadadi, R.; Rehman, M.; Lobo, R.; Chakrabarti, S.; Herrmann, J.; Lerman, A.; Grothey, A. 5-fluorouracil and cardiotoxicity: A review. *Ther. Adv. Med. Oncol.* **2018**, *10*, 175883591878014.

(3) Wigle, T. J.; Tsvetkova, E. V.; Welch, S. A.; Kim, R. B. DPYD and fluorouracil-based chemotherapy: Mini review and case report. *Pharmaceutics* **2019**, *11*, 199.

(4) Lunenburg, C. A. T. C.; Henricks, L. M.; Guchelaar, H.-J.; Swen, J. J.; Deenen, M. J.; Schellens, J. H. M.; Gelderblom, H. Prospective DPYD genotyping to reduce the risk of fluoropyrimidine-induced severe toxicity: Ready for prime time. *Eur. J. Cancer* **2016**, *54*, 40−48.

(5) U.S. Food & Drug Administration. *Table of pharmacogenetic associations*, revised May 24, 2021. https://www.fda.gov/medical-devices/precision-medicine/table-pharmacogenetic-associations.

(6) European Medicines Agency. *EMA recommendations on DPD testing priot to treamtment with fluorouracil, capecitabine, tegafur and flucytosine*; EMA/229267/2020; EMA: Amsterdam, The Netherlands, 2020. https://www.ema.europa.eu/en/news/ema-recommendations-dpd-testing-prior-treatment-fluorouracil-capecitabine-tegafur-flucytosine.

(7) Van de L'Isle, M. O.N.; Ortega-Liebana, M. C.; Unciti-Broceta, A. Transition metal catalysts for the bioorthogonal synthesis of bioactive agents. *Curr. Opin. Chem. Biol.* **2021**, *61*, 32−42.

(8) Wang, J.; Wang, X.; Fan, X.; Chen, P. R. Unleashing the power of bond cleavage chemistry in living systems. *ACS Cent. Sci.* **2021**, *7*, 929−943.

(9) Franzyk, H.; Christensen, S. B. Targeting toxins toward tumors. *Molecules* **2021**, *26*, 1292.

(10) Weiss, J. T.; Dawson, J. C.; Macleod, K. G.; Rybski, W.; Fraser, C.; Torres-Sánchez, C.; Patton, E. E.; Bradley, M.; Carragher, N. O.; Unciti-Broceta, A. Extracellular palladium-catalysed dealkylation of 5-fluoro-1-propargyl-uracil as a bioorthogonally activated prodrug approach. *Nat. Commun.* **2014**, *5*, 3277.

(11) Hoop, M.; Ribeiro, A. S.; Rösch, D.; Weinand, P.; Mendes, N.; Mushtaq, F.; Chen, X.-Z.; Shen, Y.; Pujante, C. F.; Puigmartí-Luis, J.; Paredes, J.; Nelson, B. J.; Pêgo, A. P.; Pané, S. Mobile magnetic nanocatalysts for bioorthogonal targeted cancer therapy. *Adv. Funct. Mater.* **2018**, *28*, 1705920.

(12) Völker, T.; Dempwolff, F.; Graumann, P. L.; Meggers, E. Progress towards bioorthogonal catalysis with organometallic compounds. *Angew. Chem., Int. Ed.* **2014**, *53*, 10536−10540.

(13) Pérez-López, A. M.; Rubio-Ruiz, B.; Sebastián, V.; Hamilton, L.; Adam, C.; Bray, T. L.; Irusta, S.; Brennan, P. M.; Lloyd-Jones, G. C.; Sieger, D.; Santamaría, J.; Unciti-Broceta, A. Gold-triggered uncaging chemistry in living systems. *Angew. Chem., Int. Ed.* **2017**, *56*, 12548−12552.

(14) Miller, M. A.; Askevold, B.; Mikula, H.; Kohler, R. H.; Pirovich, D.; Weissleder, R. Nano-palladium is a cellular catalyst for in vivo chemistry. *Nat. Commun.* **2017**, *8*, 15906.

(15) Bray, T. L.; Salji, M.; Brombin, A.; Pérez-López, A. M.; Rubio-Ruiz, B.; Galbraith, L. C. A.; Patton, E. E.; Leung, H. Y.; Unciti-Broceta, A. Bright insights into palladium-triggered local chemotherapy. *Chem. Sci.* **2018**, *9*, 7354−7361.
(16) Weiss, J. T.; Carragher, N. O.; Unciti-Broceta, A. Palladium-mediated dealkylation of *N*-propargyl-floxuridine as a bioorthogonal oxygen-independent prodrug strategy. *Sci. Rep.* **2015**, *5*, 9329.
(17) Weiss, J. T.; Dawson, J. C.; Fraser, C.; Rybski, W.; Torres-Sánchez, C.; Bradley, M.; Patton, E. E.; Carragher, N. O.; Unciti-Broceta, A. Development and bioorthogonal activation of palladium-labile prodrugs of gemcitabine. *J. Med. Chem.* **2014**, *57*, 5395−5404.
(18) Adam, C.; Pérez-López, A. M.; Hamilton, L.; Rubio-Ruiz, B.; Bray, T. L.; Sieger, D.; Brennan, P. M.; Unciti-Broceta, A. Bioorthogonal uncaging of the active metabolite of irinotecan by palladium-functionalized microdevices. *Chem. - Eur. J.* **2018**, *24*, 16783−16790.
(19) Lv, T.; Wu, J.; Kang, F.; Wang, T.; Wan, B.; Lu, J.-J.; Zhang, Y.; Huang, Z. Synthesis and evaluation of O2-derived diazeniumdiolates activatable via bioorthogonal chemistry reactions in living cells. *Org. Lett.* **2018**, *20*, 2164−2167.
(20) Li, B.; Liu, P.; Wu, H.; Xie, X.; Chen, Z.; Zeng, F.; Wu, S. A bioorthogonal nanosystem for imaging and in vivo tumor inhibition. *Biomaterials* **2017**, *138*, 57−68.
(21) Pérez-López, A. M.; Rubio-Ruiz, B.; Valero, T.; Contreras-Montoya, R.; Álvarez de Cienfuegos, L.; Sebastián, V.; Santamaría, J.; Unciti-Broceta, A. Bioorthogonal uncaging of cytotoxic paclitaxel through pd nanosheet-hydrogel frameworks. *J. Med. Chem.* **2020**, *63*, 9650−9659.
(22) Rubio-Ruiz, B.; Weiss, J. T.; Unciti-Broceta, A. Efficient palladium-triggered release of vorinostat from a bioorthogonal precursor. *J. Med. Chem.* **2016**, *59*, 9974−9980.
(23) Sancho-Albero, M.; Rubio-Ruiz, B.; Pérez-López, A. M.; Sebastián, V.; Martín-Duque, P.; Arruebo, M.; Santamaría, J.; Unciti-Broceta, A. Cancer-derived exosomes loaded with ultrathin palladium nanosheets for targeted bioorthogonal catalysis. *Nat. Catal.* **2019**, *2*, 864−872.
(24) Rubio-Ruiz, B.; Pérez-López, A. M.; Sebastián, V.; Unciti-Broceta, A. A minimally-masked inactive prodrug of panobinostat that is bioorthogonally activated by gold chemistry. *Bioorg. Med. Chem.* **2021**, *41*, 116217.
(25) Sánchez, M. I.; Penas, C.; Vázquez, M. E.; Mascareñas, J. L. Metal-catalyzed uncaging of DNA-binding agents in living cells. *Chem. Sci.* **2014**, *5*, 1901−1907.
(26) Tonga, G. Y.; Jeong, Y.; Duncan, B.; Mizuhara, T.; Mout, R.; Das, R.; Kim, S. T.; Yeh, Y.-C.; Yan, B.; Hou, S.; Rotello, V. M. Supramolecular regulation of bioorthogonal catalysis in cells using nanoparticle-embedded transition metal catalysts. *Nat. Chem.* **2015**, *7*, 597−603.
(27) Sabatino, V.; Rebelein, J. G.; Ward, T. R. "Close-to-release": Spontaneous bioorthogonal uncaging resulting from ring-closing metathesis. *J. Am. Chem. Soc.* **2019**, *141*, 17048−17052.
(28) Eda, S.; Nasibullin, I.; Vong, K.; Kudo, N.; Yoshida, M.; Kurbangalieva, A.; Tanaka, K. Biocompatibility and therapeutic potential of glycosylated albumin artificial metalloenzymes. *Nat. Catalysis* **2019**, *2*, 780−792.
(29) Vong, K.; Yamamoto, T.; Chang, T.-C.; Tanaka, K. Bioorthogonal release of anticancer drugs via gold-triggered 2-alkynylbenzamide cyclization. *Chem. Sci.* **2020**, *11*, 10928−10933.
(30) Ortega-Liebana, M. C.; Porter, N. J.; Adam, C.; Valero, T.; Hamilton, L.; Sieger, D.; Becker, C. G.; Unciti-Broceta, A. Truly-biocompatible gold catalysis enables vivo-orthogonal intra-CNS release of anxiolytics. *Angew. Chem.* **2021**, DOI: 10.1002/ange.202111461.
(31) Clavadetscher, J.; Hoffmann, S.; Lilienkampf, A.; Mackay, L.; Yusop, R. M.; Rider, S. A.; Mullins, J. J.; Bradley, M. Copper catalysis in living systems and in situ drug synthesis. *Angew. Chem., Int. Ed.* **2016**, *55*, 15662−15666.
(32) Wang, F. M.; Zhang, Y.; Liu, Z. W.; Du, Z.; Zhang, L.; Ren, J. S.; Qu, X. G. A biocompatible heterogeneous MOF-Cu catalyst for in vivo drug synthesis in targeted subcellular organelles. *Angew. Chem., Int. Ed.* **2019**, *58*, 6987−6992.
(33) Oliveira, B. L.; Stenton, B. J.; Unnikrishnan, V. B.; de Almeida, C. R.; Conde, J.; Negrao, M.; Schneider, F. S. S.; Cordeiro, C.; Ferreira, M. G.; Caramori, G. F.; Domingos, J. B.; Fior, R.; Bernardes, G. J. L. Platinum-Triggered bond-cleavage of pentynoyl amide and n-propargyl handles for drug-activation. *J. Am. Chem. Soc.* **2020**, *142*, 10869−10880.
(34) Du, Z.; Liu, C.; Song, H.; Scott, P.; Liu, Z.; Ren, J.; Qu, X. Neutrophil-membrane-directed bioorthogonal synthesis of inflammation-targeting chiral drugs. *Chem.* **2020**, *6*, 2060−2072.
(35) Plunk, M. A.; Alaniz, A.; Olademehin, O. P.; Ellington, T. L.; Shuford, K. L.; Kane, R. R. Design and catalyzed activation of Tak-242 prodrugs for localized inhibition of TLR4-induced inflammation. *ACS Med. Chem. Lett.* **2020**, *11*, 141−146.
(36) Chen, Z. W.; Li, H. J.; Bian, Y. J.; Wang, Z. J.; Chen, G. J.; Zhang, X. D.; Miao, Y. M.; Wen, D.; Wang, J. Q.; Wan, G.; Zeng, Y.; Abdou, P.; Fang, J.; Li, S.; Sun, C. J.; Gu, Z. Bioorthogonal catalytic patch. *Nat. Nanotechnol.* **2021**, *16*, 933−941.
(37) Dobritzsch, D.; Ricagno, S.; Schneider, G.; Schnackerz, K. D.; Lindqvist, Y. Crystal structure of the productive ternary complex of dihydropyrimidine dehydrogenase with NADPH and 5-iodouracil. Implications for mechanism of inhibition and electron transfer. *J. Biol. Chem.* **2002**, *277*, 13155−3166.
(38) Baccanari, D. P.; Davis, S. T.; Knick, V. C.; Spector, T. 5-Ethynyluracil (776C85): A potent modulator of the pharmacokinetics and antitumor efficacy of 5-fluorouracil. *Proc. Natl. Acad. Sci. U. S. A.* **1993**, *90*, 11064−11068.
(39) Blaschke, M.; Blumberg, J.; Wegner, U.; Nischwitz, M.; Ramadori, G.; Cameron, S. Measurements of 5-FU plasma concentrations in patients with gastrointestinal cancer: 5-FU levels reflect the 5-FU dose applied. *J. Cancer Ther.* **2012**, *03*, 28−36.
(40) Peters, G. J.; Lankelma, J.; Kok, R. M.; Noordhuis, P.; van Groeningen, C. J.; van der Wilt, C. L.; Meyer, S.; Pinedo, H. M. Prolonged retention of high concentrations of 5-fluorouracil in human and murine tumors as compared with plasma. *Cancer Chemother. Pharmacol.* **1993**, *31*, 269−276.
(41) European Medicines Agency. *Assessment report: Fluorouracil and fluorouracil related substances (capecitabine, tegafur and flucytosine) containing medicinal products*; EMA/274404/2020; EMA: Amsterdam, The Netherlands, **2020**. https://www.ema.europa.eu/en/medicines/human/referrals/fluorouracil-fluorouracil-related-substances-capecitabine-tegafur-flucytosine-containing-medicinal.
(42) Prior, H.; Haworth, R.; Labram, B.; Roberts, R.; Wolfreys, A.; Sewell, F. Justification for species selection for pharmaceutical toxicity studies. *Toxicol. Res.* **2021**, *9*, 758−770.
(43) Dolinsky, T. J.; Czodrowski, P.; Li, H.; Nielsen, J. E.; Jensen, J. H.; Klebe, G.; Baker, N. A. PDB2PQR: expanding and upgrading automated preparation of biomolecular structures for molecular simulations. *Nucleic Acids Res.* **2007**, *35*, W522.
(44) Li, H.; Robertson, A. D.; Jensen, J. H. Very fast empirical prediction and rationalization of protein pKa values. *Proteins: Struct., Funct., Genet.* **2005**, *61*, 704−721.
(45) O'Boyle, N. M.; Banck, M.; James, C. A.; Morley, C.; Vandermeersch, T.; Hutchison, G. R. Open Babel: An open chemical toolbox. *J. Cheminf.* **2011**, *3*, 33.
(46) Forli, S.; Huey, R.; Pique, M. E.; Sanner, M. F.; Goodsell, D. S.; Olson, A. J. Computational protein-ligand docking and virtual drug screening with the AutoDock suite. *Nat. Protoc.* **2016**, *11*, 905−919.

https://doi.org/10.1021/acs.jmedchem.1c01733
J. Med. Chem. 2022, 65, 552−561